Nonlocal van der Waals density functional: The simpler the better

Oleg A. Vydrov and Troy Van Voorhis

Articles you may be interested in

Compact two-electron wave function for bond dissociation and Van der Waals interactions: A natural amplitude assessment
J. Chem. Phys. **140**, 184108 (2014); 10.1063/1.4875338

Implementation and assessment of a simple nonlocal van der Waals density functional
J. Chem. Phys. **132**, 164113 (2010); 10.1063/1.3398840

Density functional for van der Waals forces accounts for hydrogen bond in benchmark set of water hexamers
J. Chem. Phys. **131**, 046102 (2009); 10.1063/1.3193462

Test of a nonempirical density functional: Short-range part of the van der Waals interaction in rare-gas dimers
J. Chem. Phys. **122**, 114102 (2005); 10.1063/1.1862242

Describing van der Waals Interaction in diatomic molecules with generalized gradient approximations: The role of the exchange functional
J. Chem. Phys. **107**, 7921 (1997); 10.1063/1.475105

Nonlocal van der Waals density functional: The simpler the better

Oleg A. Vydrov[a] and Troy Van Voorhis
Department of Chemistry, Massachusetts Institute of Technology, Cambridge, Massachusetts 02139, USA

We devise a nonlocal correlation energy functional that describes the entire range of dispersion interactions in a seamless fashion using only the electron density as input. The new functional is considerably simpler than its predecessors of a similar type. The functional has a tractable and robust analytic form that lends itself to efficient self-consistent implementation. When paired with an appropriate exchange functional, our nonlocal correlation model yields accurate interaction energies of weakly-bound complexes, not only near the energy minima but also far from equilibrium. Our model exhibits an outstanding precision at predicting equilibrium intermonomer separations in van der Waals complexes. It also gives accurate covalent bond lengths and atomization energies. Hence the functional proposed in this work is a computationally inexpensive electronic structure tool of broad applicability. © *2010 American Institute of Physics*. [doi:10.1063/1.3521275]

I. INTRODUCTION

In Kohn–Sham density functional theory (DFT),[1,2] only one contribution to the ground state energy is not known exactly—the correlation energy. Common approximations to the correlation energy have the form of local or semilocal density functionals.[3] One of the numerous limitations of (semi)local functionals is their inherent inability to describe such long-range correlation effects as dispersion (van der Waals) interactions.[4] Empirical dispersion corrections are quite popular and reasonably successful, but they typically entail a departure from pure DFT into the realm of classical force fields.[5] The proper physics of long-range van der Waals interactions can be captured with fully nonlocal correlation functionals.[4] However, the rigor usually comes at the cost of an explicit and cumbersome dependence on Kohn–Sham orbitals, both occupied and virtual, as exemplified by the random-phase approximation and related methods (see, e.g., Refs. 6 and 7 and references therein). An elegant compromise between rigor and computational tractability is achieved in the recently introduced class of nonlocal correlation functionals that treat the entire range of dispersion interactions in a general and seamless fashion, yet include no explicit orbital dependence and use only the electron density as input.[8–11] In this article we devise a nonlocal van der Waals functional that is considerably simpler yet more accurate than any of its precursors.[8–11] We give no derivation for the new functional form, but we show that it recovers all the relevant limits and satisfies many exact constraints. We suggest a suitable combination of exchange and correlation terms that performs remarkably well in all our benchmark tests.

II. FORMALISM

We write the nonlocal correlation energy as

$$E_c^{nl} = \frac{\hbar}{2} \int \int d\mathbf{r}\, d\mathbf{r}'\, n(\mathbf{r})\, \Phi(\mathbf{r}, \mathbf{r}')\, n(\mathbf{r}'), \tag{1}$$

where n is the total electron density. Building upon the insights gained in Refs. 10–12, and 13, we write the correlation kernel as

$$\Phi = -\frac{3e^4}{2m^2 gg'(g + g')} \tag{2}$$

with

$$g = \omega_0(\mathbf{r})R^2 + \kappa(\mathbf{r}), \tag{3}$$

and similarly

$$g' = \omega_0(\mathbf{r}')R^2 + \kappa(\mathbf{r}'). \tag{4}$$

In the above equations, $R = |\mathbf{r} - \mathbf{r}'|$ and

$$\omega_0(\mathbf{r}) = \sqrt{\omega_g^2(\mathbf{r}) + \frac{\omega_p^2(\mathbf{r})}{3}}, \tag{5}$$

with the local plasma frequency defined via $\omega_p^2 = 4\pi n e^2/m$ and the local band gap given by

$$\omega_g^2(\mathbf{r}) = C \frac{\hbar^2}{m^2} \left| \frac{\nabla n(\mathbf{r})}{n(\mathbf{r})} \right|^4, \tag{6}$$

where C is a parameter adjusted to give accurate asymptotic van der Waals C_6 coefficients, as elaborated in Sec. IV.

In the $R \to \infty$ limit,

$$\Phi \to -\frac{3e^4}{2m^2 \omega_0(\mathbf{r})\omega_0(\mathbf{r}')[\omega_0(\mathbf{r}) + \omega_0(\mathbf{r}')]R^6}, \tag{7}$$

so that E_c^{nl} of Eq. (1) has precisely the same long-range behavior as the nonlocal energy in VV09 of Ref. 11. A detailed analysis and physical justification of this asymptotic form was given in Ref. 13.

For $R \to 0$, the correlation kernel of Eq. (2) behaves as

$$\Phi = -A + B R^2 + \dots, \tag{8}$$

in accordance with the result of Koide[14] for the $R \to 0$ asymptotic behavior of the dispersion interaction energy.

a)Author to whom correspondence should be addressed. Electronic mail: vydrov@mit.edu.

In Eqs. (3) and (4), we introduced the quantity

$$\kappa(\mathbf{r}) = b\,\frac{v_F^2(\mathbf{r})}{\omega_p(\mathbf{r})} = 3\,b\,\frac{\omega_p(\mathbf{r})}{k_s^2(\mathbf{r})}, \tag{9}$$

where $v_F = (3\pi^2 n)^{1/3}\hbar/m$ is the local Fermi velocity, $k_s = \sqrt{3}\,\omega_p/v_F$ is the Thomas–Fermi screening wave vector, and b is an adjustable parameter that controls the short-range damping of the R^{-6} asymptote.

In the uniform density limit, Eq. (2) reduces to

$$\Phi^{\mathrm{uni}} = -\frac{3e^4}{4m^2}\left[\frac{\omega_p}{\sqrt{3}}\,R^2 + b\,\frac{v_F^2}{\omega_p}\right]^{-3}, \tag{10}$$

and Eq. (1) gives the following energy density per electron:

$$\varepsilon_c^{\mathrm{uni}} = 2\pi\hbar n \int_0^\infty R^2 \Phi^{\mathrm{uni}}\,dR = -\frac{3\pi^2\hbar e^4 n}{32\,m^2 v_F^3}\left[\frac{3}{b^2}\right]^{3/4}$$

$$= -\frac{e^2}{32\,a_0}\left[\frac{3}{b^2}\right]^{3/4} = -\beta, \tag{11}$$

where $a_0 = \hbar^2/me^2$ is the Bohr radius and β is a density-independent constant.

It is instructive to rewrite Eq. (10) in a different form,

$$\Phi^{\mathrm{uni}} = -\frac{9\sqrt{3}\,e^4}{4m^2\omega_p^3 R^6}\left[1 + \frac{3\sqrt{3}\,b}{(k_s R)^2}\right]^{-3}. \tag{12}$$

The above equation shows that the R^{-6} asymptote is damped at short range on the length scale given by $k_s R$.

Finally, we define our van der Waals density functional as

$$E_c^{\mathrm{VV10}} = E_c^{\mathrm{nl}} + \beta N$$

$$= \int d\mathbf{r}\, n(\mathbf{r})\left[\beta + \frac{\hbar}{2}\int d\mathbf{r}'\, n(\mathbf{r}')\,\Phi(\mathbf{r},\mathbf{r}')\right], \tag{13}$$

where $N = \int d\mathbf{r}\, n(\mathbf{r})$ is the number of electrons and β is determined by Eq. (11). By construction, E_c^{VV10} of Eq. (13) vanishes in the uniform density limit. This is a useful property: we can pair E_c^{VV10} with an existing exchange-correlation (XC) functional without affecting the description of the uniform electron gas.

It is a nontrivial task to determine how Eq. (13) behaves in the slowly varying density limit. At any rate, it has been argued that recovery of the density gradient expansion for correlation energy is of little relevance for real systems.[15]

The van der Waals functional of Eq. (13) is very simple and easily implementable. The double integral in Eq. (1) is in practice evaluated as a double sum over a numerical grid. For $R \to 0$, the kernel of Eq. (2) goes to a constant, avoiding any complications with the numerical integration. In the inner integration loop, only simple arithmetic operations need to be performed. Hence this new functional is computationally less expensive than the nonlocal functionals of Refs. 8–11.

The previous version of the nonlocal van der Waals functional, VV09 proposed by us in Ref. 11, was more computationally demanding because it used a rather elaborate damping function. Evaluation of the nonlocal correlation energy in VV09 required computing a square root, an exponent, and an error function for each pair of grid points in the double sum.

The energy derivatives, needed for the self-consistent implementation of VV09, were also quite complicated.[16] With the new VV10 model of Eq. (13), these energy derivatives are much simplified. The self-consistent implementation of VV10 within a Gaussian basis set code is described in detail in the next section.

III. IMPLEMENTATION

For the sake of brevity, in this section we switch to atomic units ($\hbar = m = e = 1$). In these units, κ of Eq. (9) is expressed rather simply as

$$\kappa(\mathbf{r}) = b\,\frac{3\pi}{2}\left[\frac{n(\mathbf{r})}{9\pi}\right]^{1/6}. \tag{14}$$

Our implementation of VV10 is very similar to the implementation of its predecessor VV09, described in Ref. 16. We express the electron density via a Gaussian basis set,

$$n(\mathbf{r}) = \sum_{\mu\nu} P_{\mu\nu}\,\chi_\mu(\mathbf{r})\chi_\nu(\mathbf{r}), \tag{15}$$

where χ_μ and χ_ν are basis functions, and $P_{\mu\nu}$ are the density matrix elements. For the self-consistent treatment, we need to find the derivatives of E_c^{VV10} with respect to $P_{\mu\nu}$,

$$\frac{dE_c^{\mathrm{VV10}}}{dP_{\mu\nu}} = \int d\mathbf{r}\, \chi_\mu(\mathbf{r})\frac{\delta E_c^{\mathrm{VV10}}}{\delta n(\mathbf{r})}\chi_\nu(\mathbf{r}). \tag{16}$$

To that end, we employ the standard formalism[17] developed for semilocal XC functionals,

$$\frac{dE_c^{\mathrm{VV10}}}{dP_{\mu\nu}} = \int d\mathbf{r}[F_n \chi_\mu \chi_\nu + 2F_\gamma \nabla n \cdot \nabla(\chi_\mu \chi_\nu)]. \tag{17}$$

We denote $\gamma = |\nabla n|^2$ for convenience. F_n and F_γ in Eq. (17) are computed as

$$F_n(\mathbf{r}) = \beta + \int d\mathbf{r}'\, n(\mathbf{r})\,\Phi$$
$$+ n(\mathbf{r})\left[\frac{\partial\kappa}{\partial n}(\mathbf{r})U(\mathbf{r}) + \frac{\partial\omega_0}{\partial n}(\mathbf{r})W(\mathbf{r})\right] \tag{18}$$

and

$$F_\gamma(\mathbf{r}) = n(\mathbf{r})\frac{\partial\omega_0}{\partial\gamma}(\mathbf{r})W(\mathbf{r}), \tag{19}$$

where

$$U(\mathbf{r}) = -\int d\mathbf{r}'\, n(\mathbf{r}')\,\Phi\left[\frac{1}{g} + \frac{1}{g+g'}\right] \tag{20}$$

and

$$W(\mathbf{r}) = -\int d\mathbf{r}'\, n(\mathbf{r}')|\mathbf{r}-\mathbf{r}'|^2\Phi\left[\frac{1}{g} + \frac{1}{g+g'}\right]. \tag{21}$$

In the above equations, Φ, g, and g' are assumed to be functions of both $\mathbf{r}$ and $\mathbf{r}'$.

Within an atom-centered basis set implementation, the gradient of E_c^{VV10} with respect to the displacement of nucleus A has three contributions,

$$\nabla_A E_c^{\mathrm{VV10}} = \mathbf{g}_{\mathrm{GBF}}^A + \mathbf{g}_{\mathrm{weights}}^A + \mathbf{g}_{\mathrm{grid}}^A. \tag{22}$$

$\mathbf{g}_{\text{GBF}}^A$ denotes the contribution of the Gaussian basis functions. This term can be evaluated by plugging F_n and F_γ into Eq. (9) of Ref. 17 instead of $\partial f/\partial n$ and $\partial f/\partial \gamma$.

The last two terms in Eq. (22) are due to the use of atom-centered numerical integration quadratures. We employ the atomic partitioning scheme of Becke,[18] which separates the molecular integral into atomic contributions,

$$E_{\text{c}}^{\text{VV10}} = \sum_A \sum_{i \in A} w_{Ai}\, n(\mathbf{r}_{Ai})$$

$$\times \left[\beta + \frac{1}{2} \sum_B \sum_{j \in B} w_{Bj}\, n(\mathbf{r}_{Bj})\, \Phi(\mathbf{r}_{Ai}, \mathbf{r}_{Bj}) \right], \quad (23)$$

where w_{Ai} and w_{Bj} are the quadrature weights, and the grid points $\mathbf{r}_{Ai}$ are given by $\mathbf{r}_{Ai} = \mathbf{R}_A + \mathbf{r}_i$, where $\mathbf{R}_A$ is the position of nucleus A, with the $\mathbf{r}_i$ defining a one-center integration grid. The quadrature weights depend on the nuclear configuration and hence have a nonzero gradient with respect to nuclear displacements,

$$\mathbf{g}_{\text{weights}}^A = \sum_B \sum_{i \in B} (\nabla_A w_{Bi}) n(\mathbf{r}_{Bi})$$

$$\times \left[\beta + \sum_C \sum_{j \in C} w_{Cj}\, n(\mathbf{r}_{Cj})\, \Phi(\mathbf{r}_{Bi}, \mathbf{r}_{Cj}) \right]. \quad (24)$$

The weight derivatives $\nabla_A w_{Bi}$ can be found in Ref. 17.

The last term in Eq. (22) arises because each one-center quadrature grid moves together with its parent nucleus and the nonlocal correlation kernel Φ depends explicitly on the distance between the grid points. The $\mathbf{g}_{\text{grid}}^A$ term can be computed as

$$\mathbf{g}_{\text{grid}}^A = \sum_{i \in A} w_{Ai}\, n(\mathbf{r}_{Ai})$$

$$\times \sum_{B \neq A} \sum_{j \in B} w_{Bj}\, n(\mathbf{r}_{Bj})\, Q(\mathbf{r}_{Ai}, \mathbf{r}_{Bj})\, (\mathbf{r}_{Ai} - \mathbf{r}_{Bj}), \quad (25)$$

where

$$Q(\mathbf{r}, \mathbf{r}') = -2\Phi \left[\frac{\omega_0(\mathbf{r})}{g} + \frac{\omega_0(\mathbf{r}')}{g'} + \frac{\omega_0(\mathbf{r}) + \omega_0(\mathbf{r}')}{g + g'} \right]. \quad (26)$$

Analytic gradients, computed via Eq. (22), enable us to perform structural optimizations routinely and efficiently.

IV. ADJUSTMENTS

$E_{\text{c}}^{\text{VV10}}$ of Eq. (13) can, in principle, be paired with nearly any existing XC functional. However, to avoid double-counting as much as possible, it is preferable to combine $E_{\text{c}}^{\text{VV10}}$ with a functional that gives no significant binding in van der Waals complexes. Since predictions of XC functionals for weakly interacting systems can differ drastically, the parameter b, controlling the short-range behavior of $E_{\text{c}}^{\text{VV10}}$, has to be adjusted for a particular parent XC approximation.

The Perdew–Wang 86 (PW86) exchange functional[19] has been shown to describe the repulsive parts of van der Waals potentials rather well,[20–22] and a refitted version of PW86 was recently proposed.[22] We denote this "refitted PW86" as

rPW86 here. In the rest of this article we will consider one particularly apt combination of the exchange and correlation terms,

$$E_{\text{xc}}^{\text{VV10}} = E_{\text{x}}^{\text{rPW86}} + E_{\text{c}}^{\text{PBE}} + E_{\text{c}}^{\text{VV10}}, \quad (27)$$

where $E_{\text{c}}^{\text{PBE}}$ is the semilocal correlation energy functional in the generalized gradient approximation of Perdew, Burke, and Ernzerhof (PBE).[23] Hereafter, we will often refer to the XC functional of Eq. (27) simply as VV10.

There are two adjustable parameters in our method, but only C in Eq. (6) affects the asymptotic dispersion C_6 coefficients. We fit C to minimize the average error for the benchmark set of 54 C_6 coefficients compiled in Tables II and III of Ref. 13. Using self-consistent electron densities from rPW86-PBE (i.e., using $E_{\text{xc}} = E_{\text{x}}^{\text{rPW86}} + E_{\text{c}}^{\text{PBE}}$), we find the optimal value of $C = 0.0093$, which gives the mean absolute percentage error (MAPE) of 14% for the whole test set of 54 species. The largest errors in C_6 occur for metal atoms. When all the metal atoms (Li, Na, Mg, Al, Zn, Ga) are removed from the benchmark set and only the remaining 48 species are considered, the MAPE in C_6 drops to 9%. Note that a slightly smaller value of the parameter C was used in Refs. 11, 13, and 16, since the source of electron densities was different.[24]

Another adjustable parameter b, introduced in Eq. (9), controls the short range damping of Φ. Using $E_{\text{xc}}^{\text{VV10}}$ of Eq. (27), we fitted b on the training set of 22 binding energies (the S22 set of Ref. 25), with the computational details described in Sec. V and the results given in Sec. VI A. We obtained the best fit with $b = 5.9$. Correspondingly, in Eq. (13) we use

$$\beta = \frac{1}{32} \left[\frac{3}{5.9^2} \right]^{3/4} = 0.00497$$

in the Hartree atomic units.

Although the rPW86 exchange functional appears to be a very good match for our correlation model, this choice is certainly not unique. In the Appendix we describe an alternative choice of exchange which is nearly equally suitable for this purpose.

V. COMPUTATIONAL DETAILS

VV10 has been implemented self-consistently into the Q-CHEM software package.[26] In our assessment of VV10, we compare its performance to another recent van der Waals functional of a similar type—vdW-DF2 of Ref. 9. Since vdW-DF2 is just a reparameterization of an earlier functional, vdW-DF of Ref. 8, we use the same implementation[27] for both of them. The full XC energy in vdW-DF2 is defined as

$$E_{\text{xc}}^{\text{vdW-DF2}} = E_{\text{x}}^{\text{rPW86}} + E_{\text{c}}^{\text{LDA}} + E_{\text{c-nl}}^{\text{vdW-DF2}}, \quad (28)$$

where $E_{\text{c}}^{\text{LDA}}$ is the correlation energy in the local density approximation, for which we use the parameterization of Perdew and Wang.[28]

All reported calculations were performed self-consistently. For weakly bound systems, the interaction energies were counterpoise corrected. The unpruned Euler–Maclaurin–Lebedev (99,590) quadrature grid was used to evaluate all local and semilocal contributions ($E_{\text{x}}^{\text{rPW86}}$, $E_{\text{c}}^{\text{PBE}}$,

and E_c^{LDA}) and the (75,302) grid was used for the nonlocal components. Deviations of computed binding energies from the reference values are analyzed with the help of mean errors (ME), mean absolute errors (MAE), and mean absolute percentage errors (MAPE). In all tables, binding energies are reported as positive values. Hence a negative ME indicates underbinding while a positive ME means overbinding.

In our recent article[16] assessing the performance of VV09, we used the same benchmark sets of weakly bound systems and the same computational details. Therefore, the results reported in Ref. 16 can be directly compared to the results obtained with the new functionals, presented in Sec. VI below.

VI. RESULTS FOR WEAKLY INTERACTING SYSTEMS

A. The S22 benchmark set

Binding energies for the S22 test set, computed with vdW-DF2 and VV10 at the geometries of Ref. 25, are given in Table I. The error statistics are summarized in Table II. Updated reference values of binding energies for the S22 set were recently obtained in Refs. 29 and 30. For our bench-

TABLE I. Binding energies (in kcal/mol) for the S22 test set. All calculations were performed self-consistently with the aug-cc-pVTZ basis set and counterpoise corrected. Molecular structures are from Ref. 25 and reference binding energies are from Ref. 29 for all systems except adenine–thymine complexes, for which the numbers from Ref. 30 were used.

Complex (symmetry)	Reference	VV10	vdW-DF2
Dispersion-bound complexes (8)			
CH_4 dimer (D_{3d})	0.53	0.50	0.68
C_2H_4 dimer (D_{2d})	1.48	1.42	1.32
Benzene–CH_4 (C_3)	1.45	1.45	1.29
Benzene dimer (C_{2h})[a]	2.66	2.71	2.15
Pyrazine dimer (C_s)	4.26	4.02	3.30
Uracil dimer (C_2)[b]	9.78	9.70	8.76
Indole–benzene (C_1)[b]	4.52	4.54	3.44
Adenine–thymine (C_1)[b]	11.66	11.42	9.58
Mixed complexes (7)			
C_2H_4–C_2H_2 (C_{2v})	1.50	1.68	1.53
Benzene–H_2O (C_s)	3.28	3.31	2.80
Benzene–NH_3 (C_s)	2.32	2.28	1.99
Benzene–HCN (C_s)	4.54	4.30	3.55
Benzene dimer (C_{2v})[c]	2.72	2.54	2.06
Indole–benzene (C_s)[c]	5.63	5.27	4.20
Phenol dimer (C_1)	7.10	6.99	5.97
Hydrogen-bonded complexes (7)			
NH_3 dimer (C_{2h})	3.15	3.43	2.97
H_2O dimer (C_s)	5.00	5.50	4.78
Formic acid dimer (C_{2h})	18.75	19.96	16.77
Formamide dimer (C_{2h})	16.06	16.71	14.43
Uracil dimer (C_{2h})[d]	20.64	21.10	18.69
2-pyridone–2-aminopyridine (C_1)	16.94	18.05	15.37
Adenine–thymine WC (C_1)[d]	16.74	17.42	14.74

[a]"Parallel-displaced" configuration.
[b]Stacked configuration.
[c]T-shaped configuration.
[d]Planar configuration.

TABLE II. Summary of deviations from the reference values of the binding energies reported in Table I. ME and MAE are in kcal/mol, MAPE is in percents.

	VV10	vdW-DF2
Dispersion-bound complexes (8)		
ME	− 0.07	− 0.73
MAE	0.09	0.76
MAPE (%)	2.6	18.0
Mixed complexes (7)		
ME	− 0.10	− 0.71
MAE	0.16	0.72
MAPE (%)	4.8	16.8
Hydrogen-bonded complexes (7)		
ME	0.70	− 1.36
MAE	0.70	1.36
MAPE (%)	6.1	8.8
Total (22)		
ME	0.16	− 0.92
MAE	0.31	0.94
MAPE (%)	4.4	14.7

mark set, we picked the values that we deemed the most converged with respect to the basis set size: we took the reference values for most of the systems from Ref. 29, except for the adenine–thymine complexes (in both stacked and planar configurations), for which we used the numbers from Ref. 30.

As Tables I and II show, VV10 performs remarkably well for all dispersion-bound and mixed complexes, but yields somewhat larger errors for hydrogen-bonded systems. The parameter b inside E_c^{VV10} was fitted to the binding energies of the S22 set, but it is by no means trivial to achieve such accuracy by adjusting just one global parameter.

vdW-DF2 overbinds some of the smaller systems, specifically $(CH_4)_2$ and C_2H_4–C_2H_2, but underbinds all other complexes in the S22 set, when the geometries from Ref. 25 are used. This underbinding tendency intensifies as the monomer sizes increase. A negative ME for the binding energies of the S22 set was also found in Ref. 9. However, intermonomer separations were optimized in Ref. 9, yielding larger binding energies, as compared to our results for the fixed[25] geometries.

Binding energies calculated for a standard set of near-equilibrium geometries certainly do not tell the full story about the performance of a functional. For a more comprehensive assessment, it is necessary to determine whether equilibrium intermonomer separations are accurately located and whether reasonable interaction energies are predicted far from equilibrium. To this end, we analyze binding energy curves for several complexes.

B. Interaction energy curves

We computed interaction energy curves for six weakly-bound systems using VV10 and vdW-DF2. Figure 1 shows the results for the argon and krypton dimers, Fig. 2 shows the results for the methane dimer (D_{3d} symmetry) and the benzene–methane complex (C_{3v}), and Fig. 3 shows the results for benzene dimers in two configurations: T-shaped (C_{2v}) and stacked sandwich-shaped (D_{6h}). We applied counterpoise cor-
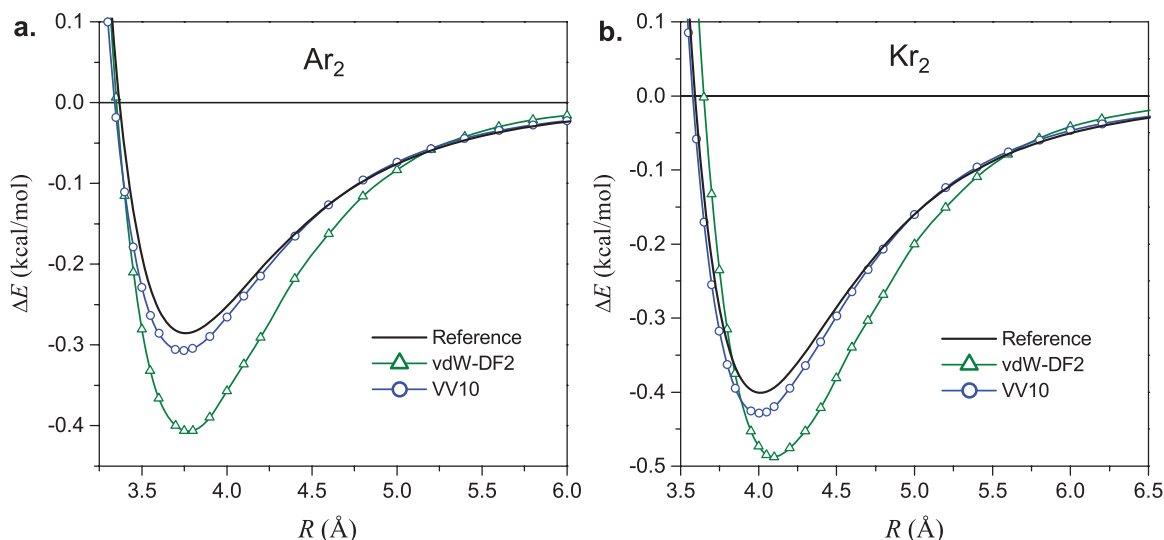
FIG. 1. Interaction energy curves for (a) the argon dimer and (b) the krypton dimer. Reference curves are from Ref. 31. VV10 and vdW-DF2 results were obtained self-consistently with the aug-cc-pVQZ basis set.
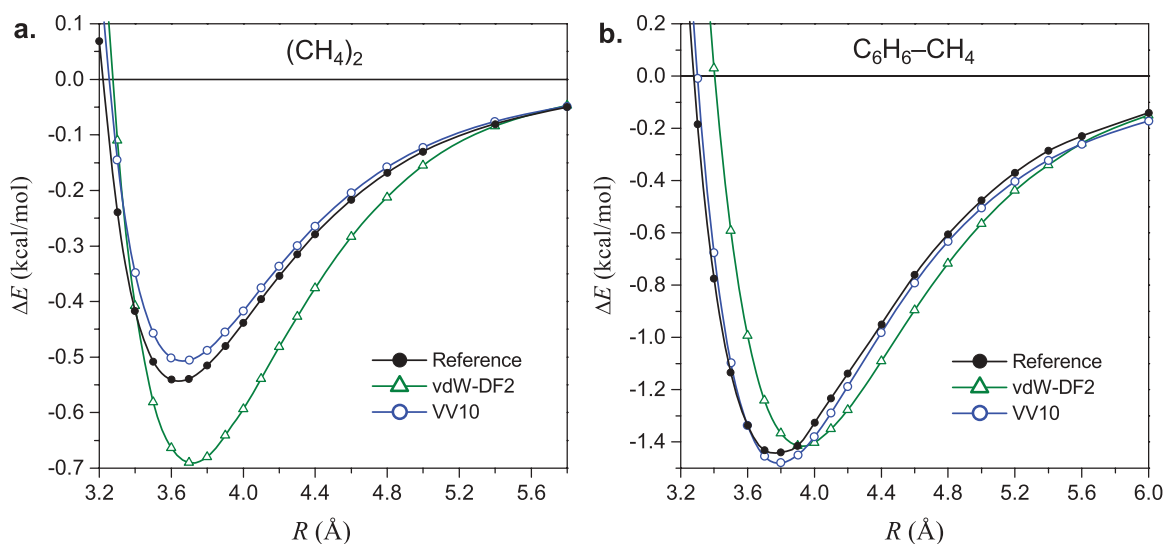

FIG. 2. Interaction energy curves for (a) the methane dimer and (b) the benzene–methane complex. R is the distance between the centers of mass of the monomers. Reference values are from Ref. 32. VV10 and vdW-DF2 results were obtained self-consistently with the aug-cc-pVTZ basis set.

FIG. 3. Interaction energy curves for (a) the T-shaped and (b) the stacked sandwich-shaped benzene dimers. R is the distance between the centers of mass of the monomers. Reference values are from Ref. 32. VV10 and vdW-DF2 results were obtained self-consistently with the aug-cc-pVTZ basis set.
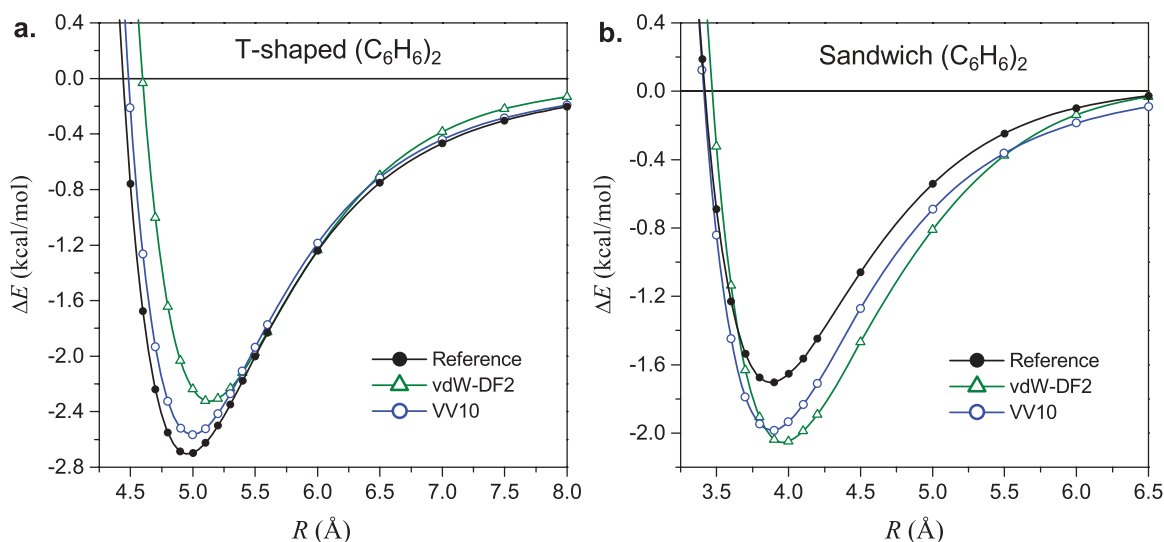
rections at all intermonomer distances. For Ar_2 and Kr_2, the reference values were taken from Ref. 31, and for the other complexes from Ref. 32. For molecular complexes, we used the same fixed monomer geometries as in Ref. 32.

For all six complexes, VV10 reproduces the equilibrium intermonomer separations with remarkable precision. Interaction energies yielded by VV10 agree quite well with the reference values at all separations. The well depths are predicted with reasonable accuracy: VV10 slightly underbinds $(CH_4)_2$ and the T-shaped $(C_6H_6)_2$, but it slightly overbinds Ar_2 and Kr_2 and more strongly overbinds the sandwich-shaped $(C_6H_6)_2$. For the benzene–methane complex, the deviations of VV10 from the reference curve are within the uncertainties of the reference[32] interaction energies at nearly all separations. The long-range falloff of the potential energy curves is reproduced very well by VV10 in nearly all cases.

vdW-DF2 tends to predict the energy minima at somewhat too large separations. It significantly overbinds the complexes of small monomers: Ar_2, Kr_2, and $(CH_4)_2$. For all systems in Figs. 1–3, except Ar_2, the repulsive walls given by vdW-DF2 are too steep and shifted toward larger distances as compared to the reference curves. As was shown in Ref. 13, vdW-DF2 strongly underestimates asymptotic C_6 coefficients. As a result, for systems where the asymptotic interactions are dominated by dispersion, vdW-DF2 will yield too shallow potential energy curves at long range. This underestimation is visible at large separations for Ar_2, Kr_2, and the T-shaped $(C_6H_6)_2$. The effects of the poor vdW-DF2 asymptotics are expected to be more noticeable at very large intermonomer distances or for very large monomers. Such cases are not significantly represented in this study.

As Fig. 3(b) shows, both VV10 and vdW-DF2 significantly overestimate the equilibrium binding energy in the sandwich-shaped benzene dimer. This may be partially caused by the lack of Axilrod–Teller-type three-body interactions in the functionals of the form of Eq. (1). Another possible source of errors is the rPW86 exchange functional. It was found in Ref. 22 that PW86 exchange is more repulsive than Hartree–Fock for the T-shaped benzene dimer, but less repulsive for the sandwich-shaped configuration.

VII. RESULTS FOR ATOMS AND COVALENT BONDS

We have shown that VV10 describes weakly-bound systems quite well. In this section, we show that VV10 is a broadly applicable method that also treats covalent and ionic bonds well.

A. Total energies of atoms

In Table III we report the total energies of atoms up to Ar, computed with rPW86-PBE (that is rPW86 exchange[22] with PBE correlation[23]) as well as VV10, which is rPW86-PBE with the addition of E_c^{VV10}, as shown in Eq. (27). We also include the popular semilocal XC functional PBE[23] We used the aug-pc-4 basis set[33] with all beyond-f polarization functions removed. This basis set is expected to yield energies close to the basis set limit. As the benchmark, we use the accurate nonrelativistic values of atomic energies from Refs. 34 and 35.

TABLE III. Total energies of atoms in Hartree atomic units. The exact values are from Refs. 34 and 35.

	Exact	PBE	rPW86-PBE	VV10
H	−0.500	−0.500	−0.509	−0.505
He	−2.904	−2.893	−2.926	−2.916
Li	−7.478	−7.462	−7.517	−7.503
Be	−14.667	−14.630	−14.709	−14.692
B	−24.654	−24.612	−24.723	−24.700
C	−37.845	−37.799	−37.941	−37.914
N	−54.589	−54.536	−54.708	−54.677
O	−75.067	−75.015	−75.230	−75.194
F	−99.734	−99.676	−99.932	−99.891
Ne	−128.938	−128.866	−129.159	−129.114
Na	−162.255	−162.172	−162.502	−162.453
Mg	−200.053	−199.955	−200.325	−200.271
Al	−242.346	−242.236	−242.645	−242.588
Si	−289.359	−289.234	−289.682	−289.621
P	−341.259	−341.115	−341.602	−341.536
S	−398.110	−397.952	−398.481	−398.411
Cl	−460.148	−459.974	−460.544	−460.470
Ar	−527.540	−527.346	−527.955	−527.876
$ME/\bar{e}$[a]		0.008	−0.019	−0.014

[a]Mean error per electron.

Among the three considered functionals, PBE gives the most accurate atomic energies. PBE total energies are systematically above the exact values, except for the H atom, for which PBE gives a nearly exact energy. On the contrary, rPW86-PBE and VV10 yield total energies that are systematically too low.

We find E_c^{VV10} of Eq. (13) to be positive not only for atoms, but for all systems considered in this study. We have no proof that E_c^{VV10} is always strictly nonnegative, i.e., that $\beta N \geq -E_c^{nl}$, but we have found no exceptions so far. The positive contribution of E_c^{VV10} brings the rPW86-PBE total energies in better agreement with the exact values, as Table III shows.

We did not include vdW-DF2 in Table III because this functional is not defined for open-shell systems. For the five closed-shell atoms in the set of Table III, vdW-DF2 yields the ME of −0.048 hartree per electron. vdW-DF2 total energies are much too low primarily because this functional includes E_c^{LDA} as a constituent and LDA is known to severely overestimate the magnitudes of correlation energies in atoms.

B. Atomization energies

We computed atomization energies for the AE6 set developed by Lynch and Truhlar.[36] This set includes only six molecules, but it is quite diverse and was constructed to be representative, that is to reproduce mean errors in much larger sets. We used the molecular geometries suggested by the authors of the set.[36] The results and the mean errors are given in Table IV.

rPW86-PBE, which is the backbone of VV10, yields considerably more accurate atomization energies as compared to the popular PBE functional. The addition of the nonlocal correlation term, E_c^{VV10}, to rPW86-PBE increases the

TABLE IV. Atomization energies for the AE6 set of Ref. 36 computed with the aug-cc-pVTZ basis set. All values are in kcal/mol.

	Reference	PBE	rPW86-PBE	VV10
S_2	101.7	112.5	106.0	108.5
SiO	192.1	193.4	190.1	191.8
SiH_4	322.4	311.6	308.2	310.2
Glyoxal	633.4	661.7	643.9	650.1
Propyne	704.8	720.1	706.1	711.5
Cyclobutane	1149.0	1166.1	1137.0	1148.8
ME		10.4	−2.0	2.9
MAE		14.0	7.4	7.2

atomization energies in all cases, as the VV10 results in Table IV show. In other words, the addition of E_c^{VV10} makes covalent bonds somewhat stronger. As a result, VV10 yields smaller errors than rPW86-PBE for three molecules in the AE6 set, but larger errors for the other three molecules. On average, the performance of VV10 for the AE6 set is quite similar to its parent functional rPW86-PBE.

C. Bond lengths

In Table V we have compiled a test set of 20 small closed-shell molecules for which experimental[37] equilibrium bond lengths (r_e) are known. The test set consists mostly of diatomics, but includes several polyatomic molecules of high symmetry whose geometry is completely determined by a single bond length. Most of the molecules in the set are covalently bound, except for the alkali metal halides where the bonding is ionic.

TABLE V. Equilibrium bond lengths (r_e) computed using the aug-cc-pVTZ basis set. All values are in Å. Experimental data are from Ref. 37.

	Expt.	PBE	rPW86-LDA	vdW-DF2	rPW86-PBE	VV10
H_2	0.741	0.751	0.734	0.736	0.745	0.745
LiF	1.564	1.583	1.592	1.592	1.586	1.585
LiCl	2.021	2.028	2.041	2.041	2.031	2.031
Li_2	2.673	2.726	2.663	2.670	2.699	2.700
CH_4	1.087	1.096	1.088	1.090	1.092	1.093
CO	1.128	1.137	1.136	1.136	1.137	1.137
CO_2	1.160	1.172	1.174	1.173	1.172	1.172
CS_2	1.553	1.566	1.573	1.571	1.568	1.567
N_2	1.098	1.103	1.101	1.101	1.102	1.102
HF	0.917	0.932	0.934	0.935	0.934	0.934
F_2	1.412	1.413	1.459	1.453	1.433	1.432
NaCl	2.361	2.385	2.410	2.401	2.390	2.385
NaBr	2.502	2.528	2.560	2.547	2.538	2.532
Na_2	3.079	3.079	3.006	2.987	3.035	3.024
SiO	1.510	1.536	1.543	1.540	1.539	1.538
P_2	1.893	1.911	1.922	1.918	1.914	1.913
HCl	1.275	1.291	1.289	1.290	1.290	1.290
Cl_2	1.988	2.019	2.085	2.073	2.040	2.037
HBr	1.415	1.433	1.436	1.437	1.435	1.435
Br_2	2.281	2.311	2.396	2.380	2.343	2.336
ME		0.017	0.024	0.021	0.018	0.017
MAE		0.017	0.033	0.031	0.023	0.022

Table V reports the results of geometry optimizations carried out using analytic gradients and the aug-cc-pVTZ basis set. We tested vdW-DF2 and VV10 alongside their semilocal parent functionals, rPW86-LDA and rPW86-PBE, respectively. We also included PBE for the sake of comparison. For most molecules in Table V, vdW-DF2 yields nearly the same bond lengths as rPW86-LDA, and VV10 nearly the same as rPW86-PBE. Hence the addition of a nonlocal correlation term has an almost negligible effect on covalent and ionic bond lengths. The largest change occurs for Na_2: the Na–Na bond length given by VV10 is 0.011 Å shorter than with rPW86-PBE. This is not surprising since the Na–Na bond is weaker than most covalent bonds. On average for the test set of Table V, the performance of VV10 is on par with PBE, while vdW-DF2 is somewhat less accurate.

VIII. CONCLUSIONS

The VV10 correlation model proposed in this work belongs to the family[8–11] of nonlocal van der Waals density functionals defined in terms of the electron density alone and using no orbital input. These functionals[8–11] are general and seamless: they require neither splitting the system into interacting fragments nor any kind of atomic partitioning. They treat inter- and intra-molecular dispersion interactions on equal footing.

VV10 has the same long-range behavior as its precursor VV09, but the damping mechanism of dispersion interactions at short range is greatly simplified in VV10. This simplification not only makes the functional more efficient and computationally tractable, but it also leads to improved overall accuracy.

An essential aspect of the VV10 formalism is the additional flexibility introduced with the help of an adjustable parameter b which controls the short range behavior of the nonlocal correlation energy. When E_c^{VV10} of Eq. (13) is added as a correction to an existing XC functional, b is adjusted to attain a balanced merging of interaction energy contributions at short and intermediate ranges. A particularly successful functional is constructed by adding E_c^{VV10} with $b = 5.9$ to rPW86-PBE, as shown in Eq. (27). Another parameter $C = 0.0093$ inside E_c^{VV10} ensures that accurate asymptotic C_6 coefficients are obtained.[24]

As our benchmark tests clearly demonstrate, the functional of Eq. (27) is a broadly accurate electronic structure tool: its outstanding predictive power for weakly-bound systems is complemented by its good description of covalent bonds.

APPENDIX: VV10 WITH LONG-RANGE CORRECTED EXCHANGE

The XC functional of Eq. (27) includes the semilocal rPW86 exchange term as a constituent. Semilocal exchange

functionals are known to suffer from self-interaction error (SIE), which causes such artifacts as poor description of charge transfer complexes and transition states of chemical reactions. Long-range corrected (LC) hybrid exchange functionals have proven to be very effective at minimizing the SIE.[38,39] LC hybrids have also been shown to adequately describe the repulsive parts of van der Waals potentials.[40] We test one particular LC hybrid for its suitability as a counterpart for the VV10 correlation model—the LC-ωPBE functional.[38,41] The exchange component in LC-ωPBE is defined as a sum of two parts: the long-range Hartree–Fock (LR-HF) part and the short-range PBE (SR-PBE) part, for which we use the parameterization of Ref. 41. For the range-separation parameter ω, we use the value of 0.45 bohr^{-1}, as suggested in Ref. 41 (this variant was termed LC-ωPBE08 therein). The full XC functional, which we denote LC-VV10, has the form

$$E_{xc}^{LC\text{-}VV10} = E_x^{SR\text{-}PBE} + E_x^{LR\text{-}HF} + E_c^{PBE} + E_c^{VV10}. \qquad (A1)$$

The two parameters inside E_c^{VV10} are adjusted using the same procedure as described in Sec. IV. As we previously found,[11,13,24] $C = 0.0089$ gives accurate C_6 coefficients at LC-ωPBE electron densities. We fit the parameter b to the binding energies of the S22 set using the functional of Eq. (A1) and obtain the optimal value of $b = 6.3$.

In Table VI we summarize the errors of LC-VV10 for the test sets used previously in this article. As compared to the VV10 model with the rPW86 exchange, LC-VV10 performs somewhat better for binding energies of hydrogen bonded complexes, for total energies of atoms, and for bond lengths. However, no improvement is observed for atomization energies, while binding energies of dispersion-bound complexes are slightly worsened on average. Therefore, we suggest using LC-VV10 only when SIE is an issue. In most other cases the VV10 model of Eq. (27) is preferable since the semilocal rPW86 exchange is computationally cheaper and much more easy to implement than an LC hybrid.

It is noteworthy that our model can achieve good performance using a pre-existing and unmodified exchange functional (rPW86 or LC-ωPBE) and adjusting only the parameters in the nonlocal correlation. It might be possible to further improve the performance by tailoring an empirical exchange functional for our specific purpose, in the vein of the recent

works of Refs. 42, 43, and 44. However, we prefer to keep empirical fitting to a minimum.

[1] W. Kohn and L. J. Sham, Phys. Rev. **140**, A1133 (1965).
[2] *A Primer in Density Functional Theory*, edited by C. Fiolhais, F. Nogueira, and M. Marques (Springer, Berlin, 2003).
[3] G. E. Scuseria and V. N. Staroverov, in *Theory and Applications of Computational Chemistry: The First Forty Years*, edited by C. E. Dykstra, G. Frenking, K. S. Kim, and G. E. Scuseria (Elsevier, Amsterdam, 2005).
[4] K. E. Riley, M. Pitoňák, P. Jurečka, and P. Hobza, Chem. Rev. **110**, 5023 (2010).
[5] S. Grimme, J. Antony, S. Ehrlich, and H. Krieg, J. Chem. Phys. **132**, 154104 (2010), and references therein.
[6] H.-V. Nguyen and G. Galli, J. Chem. Phys. **132**, 044109 (2010).
[7] W. Zhu, J. Toulouse, A. Savin, and J. G. Ángyán, J. Chem. Phys. **132**, 244108 (2010).
[8] M. Dion, H. Rydberg, E. Schröder, D. C. Langreth, and B. I. Lundqvist, Phys. Rev. Lett. **92**, 246401 (2004).
[9] K. Lee, É. D. Murray, L. Kong, B. I. Lundqvist, and D. C. Langreth, Phys. Rev. B **82**, 081101 (2010).
[10] O. A. Vydrov and T. Van Voorhis, J. Chem. Phys. **130**, 104105 (2009).
[11] O. A. Vydrov and T. Van Voorhis, Phys. Rev. Lett. **103**, 063004 (2009).
[12] D. C. Langreth and B. I. Lundqvist, Phys. Rev. Lett. **104**, 099303 (2010); O. A. Vydrov and T. Van Voorhis, *ibid.* **104**, 099304 (2010).
[13] O. A. Vydrov and T. Van Voorhis, Phys. Rev. A **81**, 062708 (2010).
[14] A. Koide, J. Phys. B **9**, 3173 (1976).
[15] J. P. Perdew, L. A. Constantin, E. Sagvolden, and K. Burke, Phys. Rev. Lett. **97**, 223002 (2006).
[16] O. A. Vydrov and T. Van Voorhis, J. Chem. Phys. **132**, 164113 (2010).
[17] B. G. Johnson, P. M. W. Gill, and J. A. Pople, J. Chem. Phys. **98**, 5612 (1993).
[18] A. D. Becke, J. Chem. Phys. **88**, 2547 (1988).
[19] J. P. Perdew and Y. Wang, Phys. Rev. B **33**, 8800 (1986).
[20] D. J. Lacks and R. G. Gordon, Phys. Rev. A **47**, 4681 (1993).
[21] F. O. Kannemann and A. D. Becke, J. Chem. Theory Comput. **5**, 719 (2009); **6**, 1081 (2010).
[22] E. D. Murray, K. Lee, and D. C. Langreth, J. Chem. Theory Comput. **5**, 2754 (2009).
[23] J. P. Perdew, K. Burke, and M. Ernzerhof, Phys. Rev. Lett. **77**, 3865 (1996).
[24] The value of $C = 0.0089$ was obtained in Ref. 11 by fitting to a C_6 test set using electron densities produced by the long-range corrected (LC) hybrid functional LC-ωPBE. As compared to LC hybrids, the description of density tails by semilocal XC functionals is systematically less accurate, which is reflected in ω_g. The readjusted value of $C = 0.0093$ is tailored for use with semilocal XC functionals, such as rPW86-PBE.
[25] P. Jurečka, J. Šponer, J. Černý, and P. Hobza, Phys. Chem. Chem. Phys. **8**, 1985 (2006).
[26] Y. Shao, L. Fusti-Molnar, Y. Jung, J. Kussmann, C. Ochsenfeld, S. T. Brown, A. T. B. Gilbert, L. V. Slipchenko, S. V. Levchenko, D. P. O'Neill, R. A. DiStasio Jr., R. C. Lochan, T. Wang, G. J. O. Beran, N. A. Besley, J. M. Herbert, C. Y. Lin, T. Van Voorhis, S. H. Chien, A. Sodt, R. P. Steele, V. A. Rassolov, P. E. Maslen, P. P. Korambath, R. D. Adamson, B. Austin, J. Baker, E. F. C. Byrd, H. Dachsel, R. J. Doerksen, A. Dreuw, B. D. Dunietz, A. D. Dutoi, T. R. Furlani, S. R. Gwaltney, A. Heyden, S. Hirata, C.-P. Hsu, G. Kedziora, R. Z. Khalliulin, P. Klunzinger, A. M. Lee, M. S. Lee, W. Liang, I. Lotan, N. Nair, B. Peters, E. I. Proynov, P. A. Pieniazek, Y. M. Rhee, J. Ritchie, E. Rosta, C. D. Sherrill, A. C. Simmonett, J. E. Subotnik, H. L. Woodcock III, W. Zhang, A. T. Bell, A. K. Chakraborty, D. M. Chipman, F. J. Keil, A. Warshel, W. J. Hehre, H. F. Schaefer III, J. Kong, A. I. Krylov, P. M. W. Gill, and M. Head-Gordon, Phys. Chem. Chem. Phys. **8**, 3172 (2006).
[27] O. A. Vydrov, Q. Wu, and T. Van Voorhis, J. Chem. Phys. **129**, 014106 (2008).
[28] J. P. Perdew and Y. Wang, Phys. Rev. B **45**, 13244 (1992).
[29] R. Podeszwa, K. Patkowski, and K. Szalewicz, Phys. Chem. Chem. Phys. **12**, 5974 (2010).
[30] T. Takatani, E. G. Hohenstein, M. Malagoli, M. S. Marshall, and C. D. Sherrill, J. Chem. Phys. **132**, 144104 (2010).
[31] K. T. Tang and J. P. Toennies, J. Chem. Phys. **118**, 4976 (2003).
[32] C. D. Sherrill, T. Takatani, and E. G. Hohenstein, J. Phys. Chem. A **113**, 10146 (2009).

TABLE VI. Errors of LC-VV10 for several test sets. LC-VV10 is defined by Eq. (A1) with $\omega = 0.45$, $C = 0.0089$, and $b = 6.3$.

	ME	MAE	MAPE (%)
S22 subsets (kcal/mol)			
Dispersion-bound	0.01	0.17	7.1
Mixed	0.09	0.16	4.0
Hydrogen-bonded	0.17	0.31	2.3
Full S22 set	0.09	0.21	4.6
Other test sets			
Energies of atoms (a.u.)	0.008[a]	0.008[a]	
AE6 (kcal/mol)	0.5	6.9	
Bond lengths (Å)	-0.006	0.014	

[a]Errors per electron.

[33]F. Jensen, J. Chem. Phys. **116**, 7372 (2002); **117**, 9234 (2002); J. Phys. Chem. A **111**, 11198 (2007); F. Jensen and T. Helgaker, J. Chem. Phys. **121**, 3463 (2004).

[34]E. R. Davidson, S. A. Hagstrom, S. J. Chakravorty, V. M. Umar, and C. Froese Fischer, Phys. Rev. A **44**, 7071 (1991).

[35]S. J. Chakravorty, S. R. Gwaltney, E. R. Davidson, F. A. Parpia, and C. Froese Fischer, Phys. Rev. A **47**, 3649 (1993).

[36]B. J. Lynch and D. G. Truhlar, J. Phys. Chem. A **107**, 8996 (2003).

[37]*CRC Handbook of Chemistry and Physics*, ed., edited by D. R. Lide (CRC Press, Boca Raton, FL, 2009)

[38]O. A. Vydrov and G. E. Scuseria, J. Chem. Phys. **125**, 234109 (2006).

[39]O. A. Vydrov, G. E. Scuseria, and J. P. Perdew, J. Chem. Phys. **126**, 154109 (2007).

[40]T. Sato, T. Tsuneda, and K. Hirao, J. Chem. Phys. **126**, 234114 (2007).

[41]E. Weintraub, T. M. Henderson, and G. E. Scuseria, J. Chem. Theory Comput. **5**, 754 (2009).

[42]K. Pernal, R. Podeszwa, K. Patkowski, and K. Szalewicz, Phys. Rev. Lett. **103**, 263201 (2009).

[43]J. Klimeš, D. R. Bowler, and A. Michaelides, J. Phys.: Condens. Matter **22**, 022201 (2010).

[44]V. R. Cooper, Phys. Rev. B **81**, 161104 (2010).